

MyROOT 2.0: An automatic tool for high throughput and accurate primary root length measurement

Alejandro González^{a,*}, Xavier Sevillano^a, Isabel Betegón-Putze^b, David Blasco-Escámez^b, Marc Ferrer^a, Ana I. Caño-Delgado^b

^a GTM – Grup de recerca en Tecnologies Media, La Salle, Universitat Ramon Llull, Quatre Camins, 30, 08022 Barcelona, Spain

^b Centre for Research in Agricultural Genomics (CRAG), Edifici CRAG – Campus UAB, 08193 Cerdanyola, Barcelona, Spain



ARTICLE INFO

Keywords:

Plant phenotyping
Root length measurement
Imaging tools
Plant science
High throughput Root phenotyping

ABSTRACT

The automatic measurement of external physical traits (i.e. phenotyping) of plant organs, such as root length –which is highly correlated with plant viability– is one of the current bottlenecks in academic and agricultural research. Although many root length measurement software tools are available to the community, plant scientists often find their usability is limited, the measurements they provide are not accurate enough or they are too limited to specific image characteristics. In response to that, this work describes MyROOT 2.0, an automatic software tool jointly developed by plant scientists and computer vision engineers to create a high throughput root length measurement tool that reduces user intervention to a minimum. Using *Arabidopsis thaliana* seedlings grown on agar plates as a case study, MyROOT 2.0 is capable of detecting the root regions of interest in a fully automatic manner with an accuracy of 98%. Furthermore, this work also presents previously unreported experiments to evaluate several constituting modules of MyROOT 2.0, such as the ability to determine image scale automatically with subpixel accuracy, or the influence of training the hypocotyl detector using wildtype or mutant samples. Finally, when compared to state-of-the-art root length measurement software tools, MyROOT 2.0 achieves the highest root detection rate, obtaining measurements which are four times more accurate than its competitors. This makes MyROOT 2.0 an attractive tool for high throughput root phenotyping.

1. Introduction

In the quest to create genetically improved crop varieties which can better adapt to future climate conditions and agricultural management techniques, plant scientists have leveraged increasingly cheaper high throughput sequencing technologies to make huge amounts of genomic data of different plant species available to the scientific community (Wetterstrand, 2017; Kuijken et al., 2015).

However, to evaluate genetic improvements it is necessary to analyze how the interaction between the genotype and the environment modifies the observable traits of the plant, a task that goes by the name of phenotyping.

When compared to the boost in genomic sequencing, the relatively slower development of phenotyping tools may hinder the advances in plant breeding and fundamental plant science (Kuijken et al., 2015). In this sense, plant scientists need high throughput tools that allow the automatic analysis of large volumes of phenotypic traits of plants grown in laboratory conditions, in order to later transfer their conclusions to agriculture.

Among all plant organs, the root is crucial for plant functioning, as some of its observable features reveal critical aspects related to plant viability (Kuijken et al., 2015). As pointed out by Wasson et al., the analysis of root system architecture (which encompasses morphological traits such as root length, root density, root branching or total root surface) is key to obtain higher crop yields (Wasson et al., 2012). This makes the root one of the best options when it comes to plant phenotyping.

For this reason, the development of automatic tools for high throughput root phenotyping constitutes one of the most significant areas of research and innovation in this field. However, many recent works in this area prove that the accurate measurement of significant root traits (like root length) is still carried out manually to a large extent (e.g. (Dresboll et al., 2013; Ytting et al., 2014; Fàbregas et al., 2018)), despite the fact that several root length measurement software tools are available to the plant science community.

This can be due to three main hurdles that plant scientists face when using available root length measurement software tools: (*i*) the ease of use (often related to the usability of the tools and the degree of manual

* Corresponding author.

E-mail address: a.gonzalez@salle.url.edu (A. González).

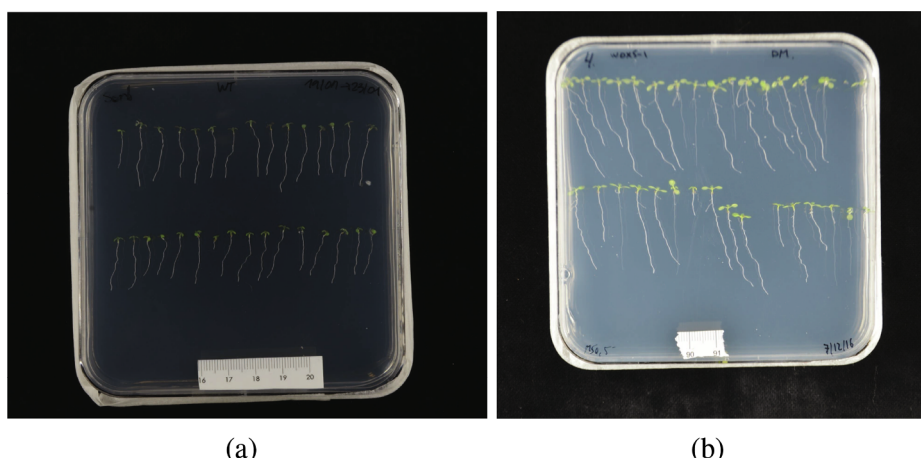


Fig. 1. Two images of *Arabidopsis* seedlings grown on an agar plate. Note that seeds were planted in two rows. Notice the differences in illumination conditions and scale.

intervention required), (ii) the constraints imposed on the image acquisition process, and (iii) the accuracy of the root length measurements.

Considering those, we recently introduced MyROOT ([Betegon-Putze et al., 2019](#)), developed as a joint effort between plant scientists and computer vision engineers to obtain an accurate and usable software tool to measure primary root length.

In that work, we tested MyROOT by measuring the primary root length of *Arabidopsis thaliana* (*Arabidopsis*) seedlings grown in agar plates (see Fig. 1), given its use as a model organism in plant science with significant implications in agricultural research.

We highlighted how its main features and usability could benefit plant scientists in need of fast and accurate primary root length measurements, providing experimental evidences of its accuracy by comparison against manual measurements made by experts. Moreover, we also analyzed how the use of MyROOT reduces labour time by half when compared to manual measurements using ImageJ. In our quest to make our tool usable and appealing to the widest possible audience among plant scientists, we identified two features that could limit their interest in MyROOT. First, the need to place a piece of measuring tape on the plate lid is not a widely used technique among plant scientists. Indeed, many image capture systems (e.g. fixed camera setups, or flatbed scanners) allow plant scientists to know the exact equivalence between pixels and centimeters. For this reason, we facilitated the introduction of this data manually through MyROOT 2.0 graphical user interface. And secondly, many plant scientists are interested in conducting measurements of many roots to validate their scientific hypotheses, which requires processing batches of images. These measurements should be processed automatically, and as quickly and efficiently as possible, saving time and effort. The previous version of MyROOT allowed batch image processing, but still required manual intervention from the user to define the region of the image where roots are located. For this reason, we have developed an automatic and efficient algorithm to detect root regions in the image, reducing manual intervention and making high throughput root length measurement feasible with MyROOT 2.0. It is important to highlight that these improvements have not made the use of the tool more complex. Moreover, the accuracy of the root length measurements remains unchanged from MyROOT to MyROOT 2.0, as the added features do not affect the measurement procedures.

To provide the reader with a comprehensive view of MyROOT 2.0 capabilities, we present a series of previously unreported experiments dedicated to the evaluation of each of the image processing algorithms that constitute the main modules of the system. Thanks to these experiments, we are able to provide a global view of the performance of the tool.

In particular, we evaluate (i) the precision of automatic image scale estimation, (ii) the accuracy of root ROI detection, (iii) the influence of wild-type and mutant models on the hypocotyl detection algorithm accuracy, and (iv) the accuracy of root length measurements, comparing them against other state-of-the-art root length measurement software tools on images provided by the authors of those.

The obtained results reveal that MyROOT 2.0 determines image scale with subpixel accuracy, and that it is capable of detecting nearly 98% of the regions of interest of the image where roots are located. Moreover, MyROOT 2.0 yields average absolute differences with respect to manual measurements four times smaller than its competitors, which makes it a very appealing alternative for plant scientists requiring accurate automatic root length measurements.

The rest of the paper is organized as follows: Section 2 reviews related work in the literature. Then, the architecture and constituting modules of MyROOT 2.0 are thoroughly described in Section 3. Section 4 presents the experimental evaluation, and finally Section 5 discusses the conclusions and proposes lines for further work.

2. Related work

The literature presents several approaches to the automatic analysis of root system architecture, mostly based on acquiring, processing and obtaining quantitative data from root images. These approaches differ on several aspects, such as (i) the medium in which the plant is grown (e.g. soil or artificial growth media like agar), (ii) the use of 2D or 3D imaging, (iii) the imaging modality (e.g. optical, X-ray, magnetic resonance, ground penetrating radar) and (iv) the degree of manual intervention required from the user.

In this section, we provide an overview of some of the most recent contributions in the area of (semi-) automated optical imaging tools developed for 2D root phenotyping in artificial media, which is the specific area of our work. The reader interested in a broader view of this topic is referred to the comprehensive survey on root phenotyping platforms by [Kuijken et al. \(2015\)](#).

The WinRHizo system is regarded as one of the pioneering efforts in the field of root phenotyping ([Arsenault et al., 1995](#)). Images captured with a scanner (which simplifies subsequent image processing due to the constant illumination conditions) were processed to obtain global root measurements (such as average root diameter, total root length or area), and also link a topology analyses of the root system architecture.

More recently, the GROWSCREEN-Root software ([Mühlich et al., 2008; Nagel et al., 2009](#)) became a relevant phenotyping tool for roots grown in Petri dishes with (semi-) transparent nutrient gel. Using infrared imaging, their image processing algorithm included nonlinear filtering and image smoothing to compensate varying background

illumination. Root lines were detected by means of local features based on steerable filters, and subsequently tracked from top to tip using a root following algorithm that took into account a correcting factor based on root orientation. The detection of crossing and branches was based on the detection of T-shaped junctions and the recursive execution of the root tracking procedure described earlier. Finally, the authors incorporated plausibility checks and/or heuristics to include temporal information to perform phenotyping of the same root along time. Based on this data, the authors extracted quantitative information of the root system architecture such as root thickness, length, orientation angle, and branch or node order.

The EZ-Rhizo software is a semiautomated tool based for measuring the length, angle and number of lateral roots, as well as the position, length and angle of lateral roots of any order (Armengaud et al., 2009). It is a heavily user driven system, as mainly consists of a user-controlled threshold-based binarization process followed by a series of noise removal operations that end up in the detection, skeletonization and manual retouching of the roots, upon which measurements are automatically made.

Focusing on tracing *Arabidopsis* seedling roots grown on agar plates, RootTrace (French et al., 2009) performs root tracing from a user-defined start location to the tip of the root. To that end, it applies the Condensation particle filter using a simple weighted color model (Isard and Blake, 1998). Following the root trace and updating the appearance model of the root as it goes, it applies a hysteresis thresholding to detect the root tip, which makes it robust against slight changes in root appearance and variations in background appearance across images. After detecting the center line of the root, RootTrace can measure the curvature of the root by calculating local angles at each point along the root trace. Recently, RootTrace capabilities were expanded to count lateral roots and the tracking model extended to recover strongly curved and agravitropic roots (Naeem et al., 2011) and put to the test in Wells et al. (2012).

In Yazdanbakhsh and Fisahn (2009), Yazdanbakhsh and Fisahn introduced PlaRoM, a hardware platform and imaging system to monitor the growth of *Arabidopsis* roots grown in agar plates, which are scanned using a camera-microscope unit mounted on a robotic arm. Their image processing algorithm allows root tip detection (Yazdanbakhsh and Fisahn, 2007), as well as measuring growth velocity profiles on time lapse records.

LeBot et al. developed DART (Le Bot et al., 2010), a software tool that relied heavily on manual labour from the user to set root markers that define root system architecture, so it should be regarded as a technical aid to visualize, organize and store the information contained in root images.

The work by Iyer-Pascuzzi et al. presented an imaging system based on gel-based growth cylinders, which were photographed at different rotation angles (Iyer-Pascuzzi et al., 2010). The image processing mainly consisted of adaptive thresholding segmentation to obtain a binary mask of the root, from which several quantitative root traits were computed (e.g. perimeter, convex area, average root radius, total length, etc.). These parameters were compacted into a feature vector that was used to train a Support Vector Machine classifier to perform classification into two rice genotypes.

SmartRoot is a software toolbox developed by Lobet et al. that allowed semiautomated image analysis for the quantitative analysis of root growth and architecture of complex root systems (Lobet et al., 2011). Using a vectorial representation of roots, SmartRoot implements a root tracing algorithm that requires the user to click anywhere along the root. The root system is treated as a collection of roots (possibly connected) that are individually represented as sets of connected segments.

GIA Roots is a semiautomated image analysis based tool that allows the calculation of up to 19 root system architecture traits (Galkovskyi et al., 2012). To that end, the image is first subjected to segmentation (either via global, adaptive or double adaptive thresholding) to separate

the root from the background. Next, the resulting binary image is optionally skeletonized, and root traits are automatically computed upon it.

The RootReader2D software (Clark et al., 2013) operated on images captured by a standard camera using a imaging setup with two cross-polarized filters to enhance the contrast of the root systems from the background, which simplified subsequent image analysis. The characteristics of the captured images made it possible to use plain thresholding to segment the root, which was then skeletonized. A connectivity analysis of the pixels of the root skeleton facilitated the detection of the root endpoints and divide the root into segments, transforming the root into a graph suitable for finding the shortest connected path between endpoints, using individual segment lengths as the graph weights.

The work by Benoit et al. (2013) constitutes an interesting contribution to one of the recurrent problems encountered when conducting root phenotyping: multiple crossing seedlings. The authors proposed using a variant of the Perona-Malik anisotropic diffusion equation to solve the segmentation at the crossings locations along the main orientations of the objects.

In Pound et al. (2013), the RootNav software was presented as a tool for the semiautomated measurement of two-dimensional root architectures. Using a top-down approach to detect roots based on EM clustering and A* search, the authors fitted a model path from root apices to the seed point, thus identifying root branches. Furthermore, the user is given the chance to manually modify the automatically traced paths.

A different approach to root phenotyping was the landmark-based root system architecture analysis presented by Ristova et al. in Ristova et al. (2013). Using a model of 20 landmarks placed manually on recognizable developmental landmarks on the root, the authors used Principal Component Analysis to distinguish between plants under different hormonal treatment conditions based on root allometry variations.

Slovak et al. introduced the BRAT software for *Arabidopsis* root phenotyping (Slovak et al., 2014). Operating on images captured through a cluster of flatbed scanners, BRAT uses SIFT features to perform alignment between the images of the same plate taken at different time instants. To detect plants, the algorithm first performs shoot detection based on color segmentation and then uses the HSV color model to detect the roots, applying a median filter for noise reduction. To detect the pixels belonging to the root, a twofold criterion that combines Sobel edge detection and background illumination variations removal is employed. Finally, roots are skeletonized, which allows computing several traits such as root length, tortuosity, growth rate, etc. BRAT can operate on a more automated or a semi-automated mode, and it needs guidance as regards the placement of the seeds.

Focusing on the specific problem of mapping nodulation patterns in legume roots, Remmler et al. designed an semi-automated algorithm to trace the primary and lateral roots of peas, although it requires intensive intervention by the user, clicking on the start and end points of the root (Remmler et al., 2014).

The work by Kumar et al. presented an imaging system combining image pre-processing for feature enhancement, feature extraction, and supervised statistical learning to perform root tip detection (Kumar et al., 2014). The proposed system first segmented the root from the background, and then applied a thinning transformation on the root. This was followed by corner detection for local feature extraction based on Zernike moments, which were fed into a Gaussian mixture model for training a statistical classifier. This type of classifier performed a hierarchical classification of the detected corners into root tip (distinguishing between primary and lateral root tips) and non-root tips.

RootGraph was a root analysis software structured as a four-step pipeline comprising segmentation, distance transform, skeletonization and graph computation (Cai et al., 2015). At its latter stage, RootGraph uses graph optimization algorithms to automatically separate lateral

and primary roots, estimating several phenotypic root traits such as length and diameter.

More recently, the PlantRoot imaging system was presented in the context of the RhizoChamber-Monitor robotic platform for root growth patterns grown in rhizoboxes (Wu et al., 2018). That software allowed to analyze the spatiotemporal dynamics of root growth from time-course images of multiple plants, quantifying growth traits of primary and lateral roots (length and diameter) in a dynamic manner.

What are the main advantages of MyROOT 2.0, when compared to other existing root length measurement software tools? First, MyROOT 2.0 operates on photographs of agar plates imaged from a top perspective with a standard digital camera or even a good quality cell phone, with no need for special nor expensive imaging equipment (such as camera-microscope units mounted on a robotic arm (Yazdanbakhsh and Fisahn, 2009) or an array of flatbed scanners¹ (Slovak et al., 2014)). Second, MyROOT 2.0 requires no manual effort from its users to complete root length measurements, with no need for pinpointing individual features of each and every one of the roots under analysis (e.g. as in French et al., 2009; Remmert et al., 2014). Third, MyROOT 2.0 is capable of accurately estimating image scale from the analysis of a piece of measuring tape stuck on the plate lid. Furthermore, MyROOT 2.0 ensures accurate root length measurement by detecting the root start and end points, while other systems merely detect the plant shoot to define the root start point, which is incorrect from a biological point of view (Armengaud et al., 2009; Slovak et al., 2014).

3. Description of MyROOT 2.0

MyROOT 2.0 is designed as a three-stage image processing pipeline comprising (i) the detection and analysis of the measuring tape to infer image scale, and the roots (ii) segmentation and (iii) measurement. Fig. 2(a) depicts the schematic block diagram of MyROOT 2.0 pipeline, while Fig. 2(b) represents the image regions in which the processing of each pipeline stage takes place.

The following paragraphs summarize the operations performed on the input image. First, MyROOT 2.0 automatically detects the measuring tape regardless of its position on the plate. Next, it analyzes the region corresponding to the tape, detecting the millimeter lines and performing rotation corrections if necessary, extracting the pixel-to-millimeters equivalence corresponding to the image.

Next, the analysis focuses on the roots. MyROOT 2.0 first detects the seedlings rows in the plate, finding the root region of interest (root ROI) that contains each row of roots to be measured. Then, the roots enclosed in these ROI are segmented from the background. Subsequently, each root is tracked upwards from its tip to its starting point, the position of which is defined by the detection of each root's hypocotyl. As a result, roots can be traced and their length measured.

Finally, the measurement results are output as an image indicating the length in millimeters of each root. Furthermore, these measurements are also transferred to RSML, Excel and text files to facilitate subsequent analysis.

The following sections present a thorough description of the methods and algorithms that implement the processes just outlined.

3.1. Measuring tape detection and analysis

The first stage of the pipeline aims at automatically detecting the measuring tape placed on the plate lid for determining the conversion factor between pixels and millimeters for the given input image, which is a key issue for reporting accurate root measurements. Fig. 3 shows

¹ It is fair to mention that these software tools are also able to process images taken by other means. However, their image analysis algorithms are highly adapted to the extremely stable visual characteristics of flatbed scanner images, offering little adaptability to process different types of images satisfactorily.

the schematic diagram of this module.

Taking into account the luminance contrast between the measuring tape and the background, we search for a white patch in the image. To do so, we compute the Radon transform of the image at 0 and 90 degrees to obtain its 1D projections onto the vertical and horizontal axes. However, the edges of the plate often show high luminance in the image, which may lead to spurious peaks in these projections. For this reason, we apply median filtering on them to soften such peaks and thus, avoid confusing these regions with the measuring tape.

Next, finding the widest regions with maximum value in both projections allows finding the bounding box of the measuring tape. The inner side of this bounding box is the region of interest which is processed to ultimately obtain the pixels-to-millimeters equivalence.

To that end, we search for the centimeters marks on the tape by first segmenting the region of interest using Otsu's method. Then, we apply the morphological bottom-hat operator to remove the millimeter marks. To compensate for slight slants occurred at the time of sticking the measuring tape on the agar plate lid, we apply the Hough transform for line detection to determine the predominant orientation of the centimeter marks, and subsequently rotate the image by the negative of that angle to ensure the vertical orientation of the centimeter marks. Next, we compute the 1D Radon transform at 90 degrees to obtain a horizontal projection of the marks on the measuring tape. On this projection, we apply a local maxima finding algorithm to find the median separation between consecutive centimeter marks, which is used to compute the pixels-to-millimeters conversion factor.

3.2. Root segmentation

The root segmentation module aims at separating pixels that belong to the roots from pixels in the background. The processes followed to achieve this goal are represented in the block diagram depicted in Fig. 4.

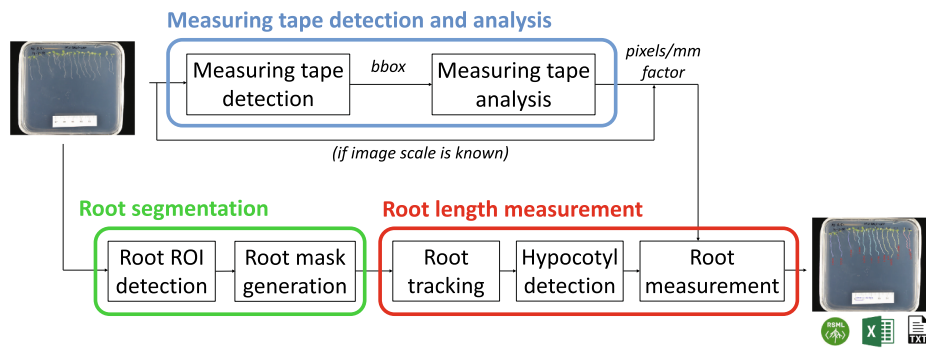
3.2.1. Root ROI detection

The root segmentation process starts by detecting the seedling rows in the plate. The roots of each seedling row are considered to belong to a root region of interest (ROI). Thus, the detection of root ROI consists of two main steps: (i) detection of seedling rows, and (ii) determination of each root ROI bounding box.

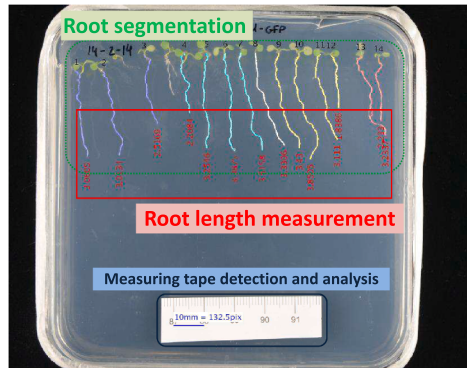
To detect seedling rows, the inner plate region is first automatically cropped by detecting plate borders using adaptive thresholding. Then, the resulting image is segmented in the RGB space to detect the green leaves of the seedlings, considering as leaf pixels all those in which the green channel takes the highest value (see Fig. 5(a)). After applying morphological opening to remove noisy detections, we compute the horizontal projection of the binary image corresponding to the leaves. On this projection, we detect local maxima to determine the number of seedling rows.

Moreover, from this projection we define the upper edge of the bounding box (or boxes) enclosing the root ROI in the plate. Also, the vertical projection of the same binary image enables us to define the right and left edges of the root ROI bounding boxes.

Finally, using the aforementioned edges to obtain subimages corresponding to each root ROI, we apply Otsu's method to perform a preliminary detection of the roots. The goal of this step is to find the longest roots in the ROI to define the bottom edge of the bounding box. This is accomplished by applying a triple noise reduction process: first, morphological opening is applied to remove noisy isolated pixels corresponding to plate lid scratches or droplets. Then, connected components with non-vertical orientation are also removed. Then, the horizontal projection of the resulting binary image is subjected to a uniform quantization process to eliminate noisy detections. Finally, the first zero after the largest peak of the quantized projection is used to define the vertical coordinate of the bottom edge of the bounding box (see Fig. 5(b)).



(a) MyROOT 2.0 pipeline block diagram



(b) MyROOT 2.0 key processing regions

Fig. 2. Block diagram and key processing regions of MyROOT 2.0.

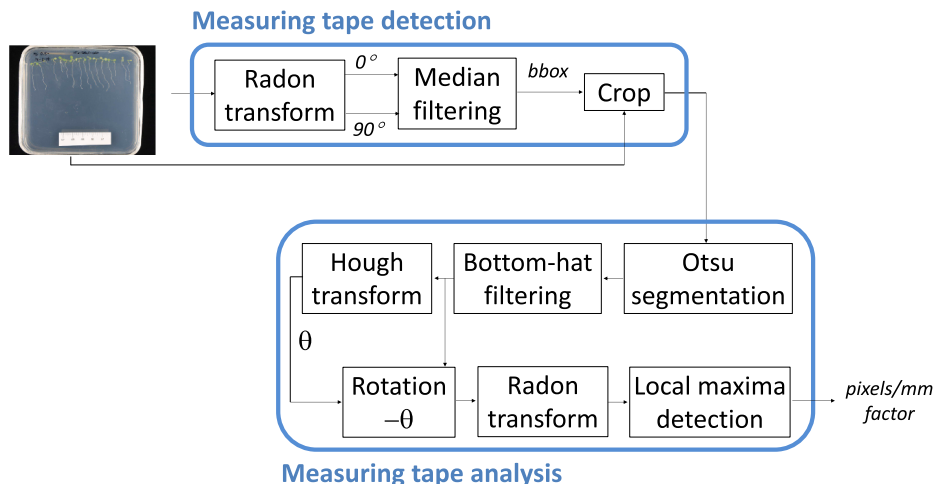


Fig. 3. Block diagram of the measuring tape detection and analysis module.

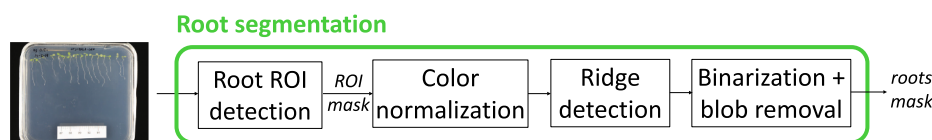


Fig. 4. Block diagram of the root segmentation module.

As a result, MyROOT 2.0 presents the input image with the detected bounding boxes superimposed (see Fig. 5(c)). The vertices of the bounding boxes are dragable, so the user can modify the detected root ROI. Moreover, it is also possible to add a new root ROI in an entirely manual manner if necessary.

3.2.2. Root detection and segmentation

From this point, the goal is creating the root mask, i.e. a binary mask for each root ROI in which root pixels are represented in white and background pixels, in black.

In an attempt to make MyROOT 2.0 useful under a wide range of

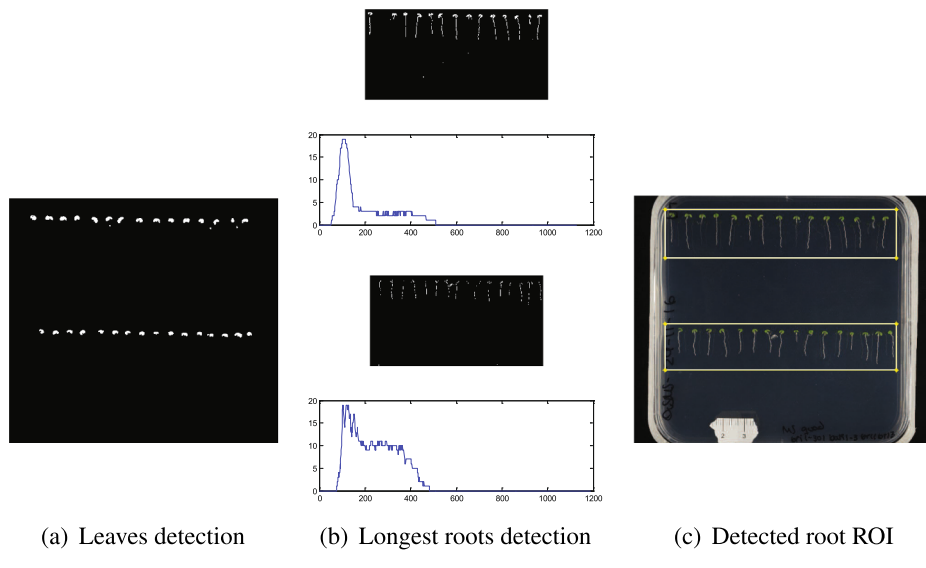


Fig. 5. Root ROI detection steps.

image acquisition conditions (e.g. different illuminant types, or changes in camera settings), we aim at making the root segmentation process robust to these variations by first conducting a color normalization step. Taking into account that roots and leaves are typically whitish and greenish, respectively, we apply a transformation that makes these colors contrast with the dark background to simplify the subsequent segmentation steps. This transformation consists in converting the image to the HSV color model and obtaining a hue-independent new version of the image by combining the saturation and value channels as $(1 - S) * V$.

Next, we perform root detection which not only considers the intensity of root pixels, but also considers the topological structure of the roots with respect to their surroundings. Indeed, as roots have a tubular structure (e.g. similar to blood vessels), we use ridge detection for determining which pixels correspond to the roots. To that end, we compute the local blockwise standard deviation of the color normalized image at a 5x5 pixels scale.

Finally, we must take into account that false ridge detections may occur caused by scratches, root reflections or condensation droplets on the plate lid. For this reason, we finally apply a binarization on the image obtained from the ridge detection, and remove small connected components to get rid of noisy detections. As a result, a binary mask

corresponding to the roots is obtained.

Fig. 6 presents the results of the color normalization, ridge detection and binarization processes just described.

3.3. Root measurement

This module takes the mask generated by the roots segmentation block described in the previous section and conducts the individual measurement of each root.

To measure root length, three sequential processes are conducted: root tracking, hypocotyl detection and root measurement.

3.3.1. Root tracking

First, root tracking aims at providing a complete list of pixels belonging to each root. In this work, we propose a bottom-up tracking approach that searches for white blobs upwards row by row, starting from the root tip and finishing at the line traced after the hypocotyl detection process (described in Section 3.3.2).

The tracking process assumes constant velocity (i.e. soft constant changes in position). Using variable t to refer to rows, the position of a track in the next state (i.e. row) is predicted as $\bar{x}_t = x_t + V_x$, with velocity $V_x = \chi_{t+1} - \chi_t$.

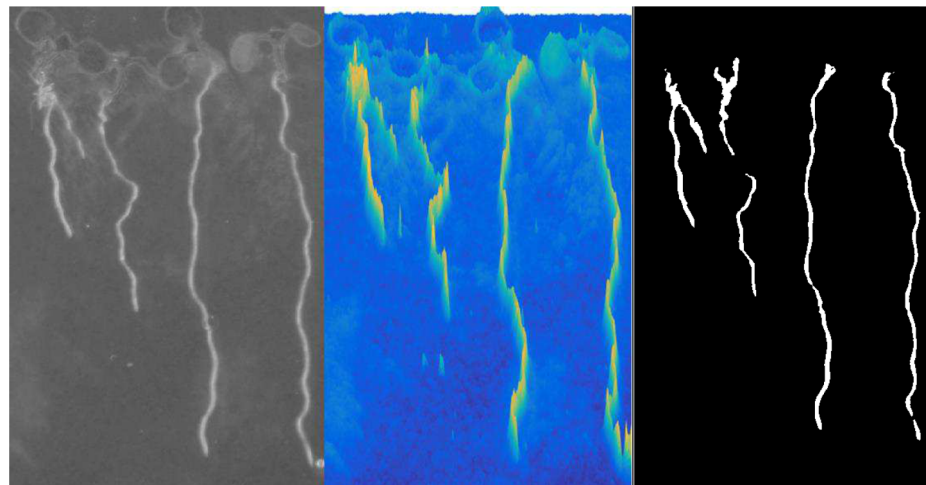


Fig. 6. Root segmentation intermediate steps: color normalization, ridge detection and binarization. (For interpretation of the references to colour in this figure legend, the reader is referred to the web version of this article.)

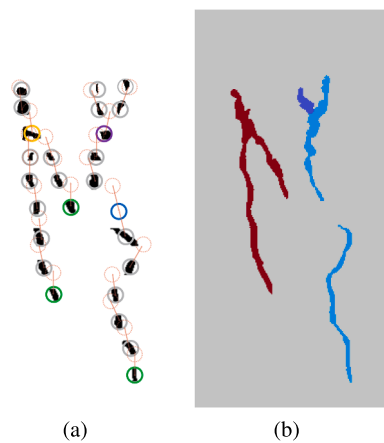


Fig. 7. Root tracking intermediate steps: (a) bottom-up tracking, and (b) root identification (right).

The tracking process starts at the lowest row of the image where at least one root is detected. We refer to this detection as d_k^t , where t refers to the row and k refers to the root. These detections are depicted as green circles in the lowest part of Fig. 7(a). Upon each new detection, a new root (χ_k^t) is generated, and it is assigned a zero initial velocity ($V_{\chi_k} = 0$), and a predicted position equal to its original position ($\tilde{\chi}_k^t = \chi_k^t$). At this point, all the created roots –namely n – are collected creating the root track set ($\mathcal{R} = \{[\chi_1^t, V_{\chi_1}, \tilde{\chi}_1^t]; \dots; [\chi_n^t, V_{\chi_n}, \tilde{\chi}_n^t]\}$).

The next step of the tracking consists in detecting white blobs in the next row (d^{t+1}). Then, using a matching process based on distance we pair detections with predictions ($d^{t+1} \Rightarrow \tilde{\chi}^t$), which are represented by dashed red circles and arrows in Fig. 7(a). As a result of this matching process, three main different situations may be encountered:

- **Correct match:** the detection is matched to a existing root (indicated by gray circles in Fig. 7(a)). In this case, the values of the current state of the root (velocity and predicted position) are updated ($\chi = d, V_\chi = \chi_{t+1} - \chi_t, \tilde{\chi}^{t+1} = \chi^t + V_\chi$).
- **Missed match:** this means that one of the existing roots (χ_k) does not match with any detection (depicted as blue circles in Fig. 7(a)). In this case, the prediction is assigned as current state ($\chi_k = \tilde{\chi}_k$), while velocity and prediction are updated ($V_{\chi_k} = \chi_k^{t+1} - \chi_k^t, \tilde{\chi}_k^{t+1} = \chi_k^t + V_{\chi_k}$).
- **Missed detection:** this happens when the current detection (d_k) does not match with none of the existing roots (shown as green circles in Fig. 7(a)). This means that a new root has been found, so it is added to our root set ($\mathcal{R} = [\mathcal{R}; [\chi^t = d_k, V_\chi = 0, \tilde{\chi}^t = d_k]]$).

During the root tracking process, two more special cases may occur. First, when a current root matches with more than one detection, which happens when a split occurs (purple circle in Fig. 7(a)). In this case, we create a new root sharing the same historical record as the *old* one. And second, when two roots converge and, consequently, they both match with a single detection (yellow circle in Fig. 7(a)). In this situation, the shortest root is eliminated from the root set and is added as a sub-root of the longest one.

Finally, using the detections history we can determine which pixels belong to each root, thus completing the root identification process (Fig. 7(b)).

3.3.2. Hypocotyl detection

As mentioned earlier, the hypocotyl is the stem of a germinating seedling, found below the cotyledons (seed leaves) and above the radicle (root). During the first days of germination, the hypocotyl is clearly visible as a brownish oval in the junction between the leaves and the root. In later stages of plant development, the growth of the leaves



Fig. 8. Regression curve (in blue) traced after the detection of hypocotyls (represented by black circles). (For interpretation of the references to colour in this figure legend, the reader is referred to the web version of this article.)

hides the hypocotyl, although its position in space is invariant along time. Thus, its detection allows setting the start point of the roots.

However, the shape and appearance of hypocotyls may vary from one seedling to another. For this reason, as in this work we assume that seedlings are placed in rows, the detection of a few hypocotyls will enable us to trace a regression curve to estimate the position of the non-detected ones. The intersection between the regression curve and each root will be used as the point at which the root will be *cut* (in terms of length measurement), as illustrated in Fig. 8.

To detect the hypocotyls, we follow a classic object detection approach based on learning the visual characteristics of the hypocotyls by training a supervised classifier on a labeled set of images containing positive and negative examples. In particular, we propose extracting visual image features to learn color and appearance models –using Histograms of Oriented Gradients (HOG) (Dalal et al., 2005) as the appearance descriptor, and color histograms as the color descriptor–, plus using a linear Support Vector Machine (linSVM) as the classifier.

To train the hypocotyl detector, we use a manually annotated hypocotyl positive and negative examples to learn the color and appearance models (see Fig. 9 for a few samples of the positive examples).

To compute appearance and color descriptors, a 48×48 pixels sample window is divided in regular not overlapping 8×8 pixels cells. The HOG descriptor is obtained by concatenating and normalizing histograms of gradient orientations computed inside each cell, while the color descriptor consists in concatenated color histograms (one per channel) computed using the same cells distribution. The color and appearance descriptors are used to train the linSVM classifier, which learns the max-margin hyperplane that better splits these samples in the descriptor space.

Once the detector is trained, we can proceed to detect hypocotyls on the input image. Using a sliding window approach, an exhaustive search of hypocotyls is conducted. Finally, while maintaining the



Fig. 9. A few positive examples used for training the hypocotyl detector.

highest scored windows as true detections, we define a hypocotyl detection curve using polynomial regression.

3.3.3. Root measurement

Once the root tracking process is completed and the hypocotyl detection regression curve is traced, each root is measured based on its tracked previous positions.

We first compute the root length in pixels by adding the distances between consecutive positions, and then obtain the actual root length by multiplying the pixel length by the pixels-to-millimeters conversion factor.

Next, we apply a two-stage refinement process: in the first step, those roots that have been tracked beyond the hypocotyl regression curve are cut at the point where the curve intersects the root, updating the length.

And in the second step, we remove *unwanted* roots. This can be done in two ways: (i) we can remove *noisy* roots, i.e. those roots which are a percentage shorter than the longest measured root, as usually roots on a plate tend to have similar lengths, and (ii) we can remove any root at will if, for some reason, the user considers it should be excluded from the measurement.

Fig. 10 illustrates the different stages of the root length measurement refinement process just described. Starting with the measurements presented in Fig. 10(a), roots are first cut at the hypocotyl regression curve length (see roots #4, #5 and #6 in Fig. 10(b)). Then, the user can select removing any root from the analysis, such as root #3 in Fig. 10(c).

Finally, as a unique identifier is given to each root, and the individual root length measurement results are stored in RSML, Excel and plain text files for subsequent analysis. Moreover, a labeled version of the input image presenting the root identifiers and the length measurements is also generated and saved (see Fig. 11).

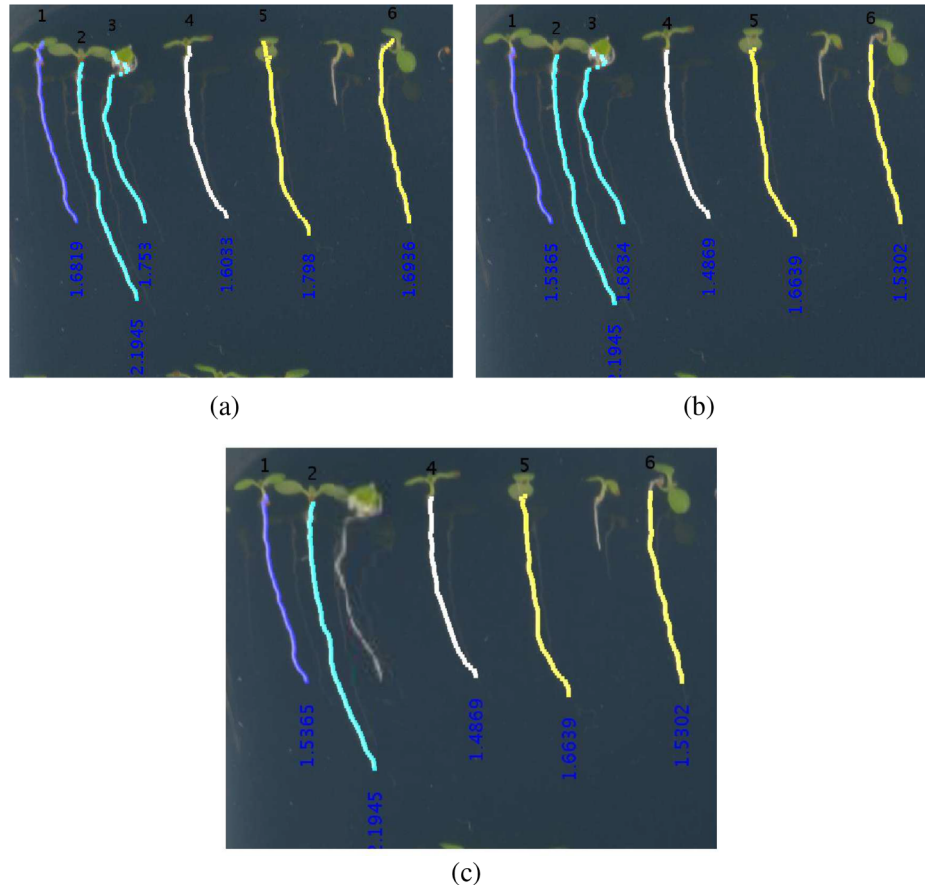


Fig. 10. Root length measurement refinement steps: (a) original image, (b) root cut at hypocotyl regression curve, and (c) root removal.



Fig. 11. Results of the individual roots measurements.

4. Experiments

This section presents a series of experiments oriented to evaluate different aspects of the algorithms that implement MyROOT 2.0. First, we describe the set of images of agar plates with *Arabidopsis* seedlings used for conducting the experiments. Second, we present an experiment in which the precision of the automatic detection and analysis of the measuring tape is tested. Third, we evaluate the root ROI detection process. Next, we analyze the accuracy of the hypocotyl detection algorithm by training the detector upon different color and appearance models built using wild-type and mutant hypocotyls. And finally, we present an experiment that compares the root length measurements obtained by MyROOT 2.0 with the measurements obtained by two state-of-the-art software tools: BRAT and EZ-Rhizo.

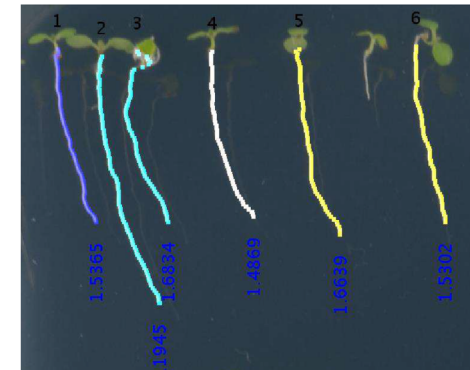


Fig. 12. Precision of the automatic detection and analysis of the measuring tape.



Fig. 13. Root ROI detection process.

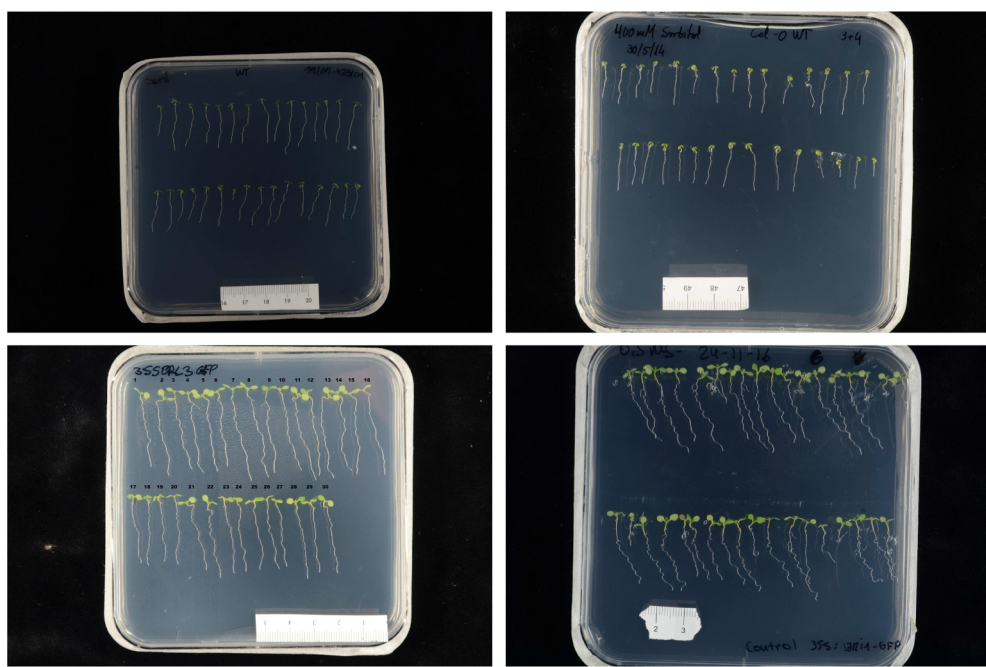


Fig. 12. Samples of the set of images taken by the plant scientists in our team used for evaluating MyROOT 2.0.

Table 1
Average manual vs. MyROOT 2.0 pixels-to-centimeter equivalence (in pixels).

Plate	Manual	MyROOT 2.0	Absolute difference
1	226.32	226.67	0.35
2	244.00	243.33	0.67
3	237.00	235.00	2.00
4	254.00	253.33	0.67
5	232.00	231.67	0.33
6	209.19	206.67	2.52
7	233.00	231.67	1.33
8	229.50	230.00	0.50
9	283.57	281.67	1.90
10	217.00	216.67	0.33
11	268.09	265.83	2.26
12	269.33	269.17	0.16
13	255.71	253.33	2.38
14	276.31	276.67	0.36
15	241.43	240.00	1.43
16	248.50	248.33	0.17
17	250.13	250.00	0.13
18	215.26	215.00	0.26
19	215.65	215.83	0.18
20	215.59	215.00	0.59

4.1. Image data and experimental setup

In order to validate the proposed framework, a set of 120 images with 4928×3264 resolution was acquired by the plant scientists in our team using a D7000 Nikon camera. To take the pictures, the agar plates were laid on a dark surface and a measuring tape at least 1 cm long was placed on them. The images were taken on different days by different users, always from a top perspective and under slightly different conditions as regards distance and illumination. The images shown in Fig. 12 represent a small sample of such pictures. We have selected several subsets of these images to conduct the experiments described in the forthcoming sections.

As for the setup of the agar plates, the *Arabidopsis* seedlings have been arranged in one or two rows of around 15 seeds each. The seedlings have been grown in lab conditions (controlled illumination, temperature and humidity) during a period of time ranging from three

to eight days, which allows not only conducting *instant* root length measurement experiments, but also performing *continuous* root length measurements of growing roots during successive days.

Finally, the manual measurements conducted by expert plant scientists, they have been completed using the ImageJ open source image processing program (Schindelin et al., 2015).

4.2. Automatic image scale from measuring tape detection and analysis

This first experiment evaluates the accuracy of MyROOT 2.0 to automatically determine the image scale from the detection and analysis of the measuring tape. To that end, a set of 20 images was processed both by means of MyROOT 2.0 and manually by at least three expert plant scientists to obtain the equivalence between pixels and one centimeter. To obtain the equivalence manually with ImageJ, a line was drawn over one centimeter of the measuring tape in the image. Then, using the *Analyze* → *Set scale* menu option of ImageJ, the distance of that line was set as the equivalent to 10 mm.

To test the robustness of the measuring tape detection and analysis algorithms against changes in image characteristics, images with different scales and illumination conditions were selected, and also with different placement, size and orientation of the measuring tape (see Fig. 12).

Table 1 presents the pixels-to-centimeter equivalences obtained by manual measurements (average of values obtained by the plant scientists who did the experiment) and by means of MyROOT 2.0. It can be observed that the absolute difference between measurements is smaller than 1 pixel in 13 of the 20 plates, and only in 3 of the 20 plates this difference is larger than 2 pixels. The correlation coefficient between manual and MyROOT 2.0 measurements is 0.999.

On average, the average absolute difference between manual and MyROOT 2.0 measurements is 0.93 pixels. This means that MyROOT 2.0 attains subpixel precision at determining the pixels-to-centimeters equivalence from the analysis of the measuring tape placed on the plate lid.

It is interesting to note that, in order to obtain satisfactory results, the *Ruler Threshold (RT)* parameter had to be tuned for a few of the images in the testbed, depending on the illumination conditions. For most of them, the default $RT = 0.7$ value was adequate. However, this

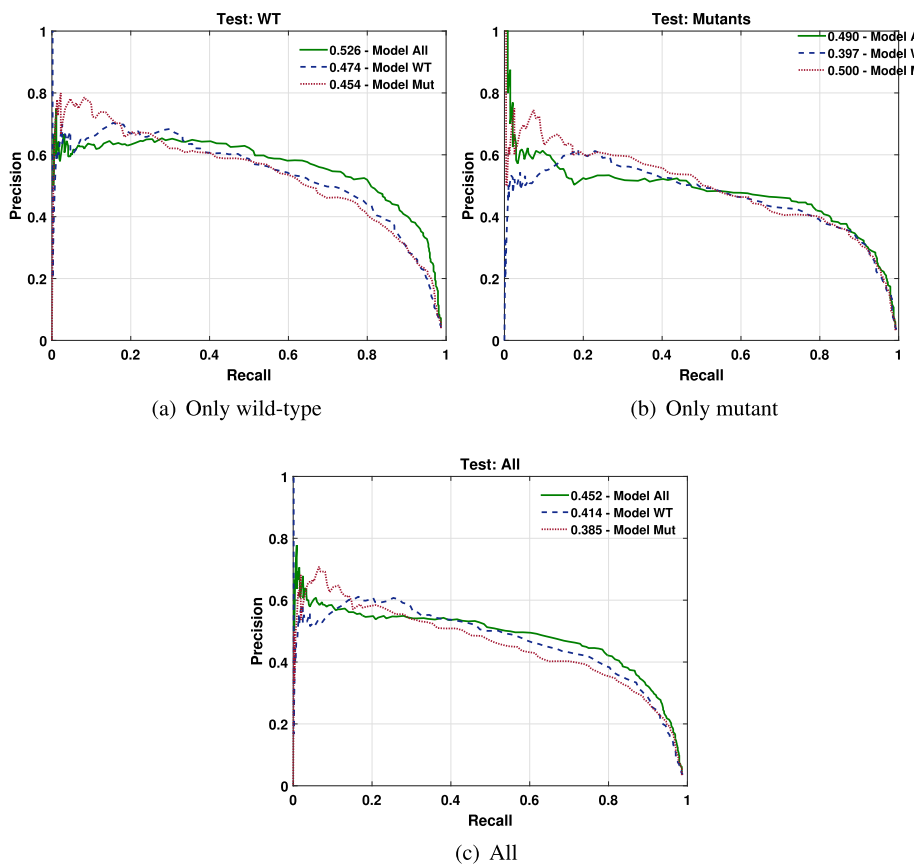


Fig. 13. Precision-Recall curves of the hypocotyl detection experiments.

parameter had to be increased (typically to $RT = 0.9$) for more brightly illuminated images, or decreased to $RT = 0.5$ for darker images.

4.3. Root ROI Detection

In this experiment, we evaluate the automatic detection of the roots ROI. To that end, we selected a set of 45 images in which seedlings were arranged in one or two rows, which are the most common way plant scientists place seedlings on Petri dishes for their experiments. In particular, 20 images contained one row of seedlings, while the 25 remaining images contained two rows, which amounts to a total 70 root ROI. Moreover, these images were taken by different plant scientists at different points in time, so they vary in terms of illumination conditions and distance to the camera. This enabled us to test the algorithm in a wide range of situations.

We first evaluate the accuracy of the algorithm to determine the correct number of seedling rows in each image. In 44 of the 45 images, the correct number of seedling rows is detected. The only error occurred in an image containing two rows, but only one was detected because it contained less than half the seedlings of the other and did not surpass the predefined threshold to be considered as a row. However, as mentioned earlier, MyROOT 2.0 allows the user to define root ROI manually after the automatic detection, so this infrequent problem can be circumvented.

Next, we evaluate if the root ROI bounding boxes automatically generated by MyROOT 2.0 contain *all* the *complete* roots of the corresponding seedling row. This is an important metric as regards the ability of MyROOT 2.0 to provide an automatic segmentation of the regions of interest of the image without user supervision.

The obtained results show that 98.6% of the detected root ROI contained all the roots in the corresponding seedling row. Moreover, 92.9% of the root ROI contained the complete roots, and only in a few

cases did the longest roots extend beyond the limits of the bounding boxes.

These results highlight that the root ROI detection module is capable of providing a highly accurate segmentation of the regions of interest in the image in a fully automatic manner. However, thanks to the interactive design of MyROOT 2.0, a user that was not satisfied with the detected root ROI could easily add additional ROI or modify the shape of the detected ones, and proceed with the analysis.

4.4. Hypocotyl detection

This experiment evaluates the algorithm designed for setting, in an automatic manner, the starting point of each root by means of hypocotyl detection. In particular, we evaluate the performance of the detector depending on the morphological differences of hypocotyls caused by different gene expression patterns, a typical situation encountered in plant science.

To that end, we selected a set of 47 images containing hypocotyls with varied morphologies: wild-type and mutant (long, short and dwarf). These images were manually annotated to define the bounding boxes of the hypocotyls to generate positive examples to train the hypocotyl detector and also to test its performance. In total, 1737 hypocotyls were annotated (907 wild-type and 830 mutants), which were also flipped to obtain a total 3474 positive examples.

These examples were divided into a training and a test set comprising 958 hypocotyls (530 wild-type and 428 mutant) and 779 hypocotyls (377 wild-type and 402 mutants), respectively.

The training examples were used to build detection models of (i) only mutant, (ii) only wild-type, and (iii) all (mutant plus wild-type), which were tested to detect only mutant, only wild-type, and mutant plus wild-type hypocotyls. By doing so, we evaluate how hypocotyl appearance variability caused by genetic mutations affects the

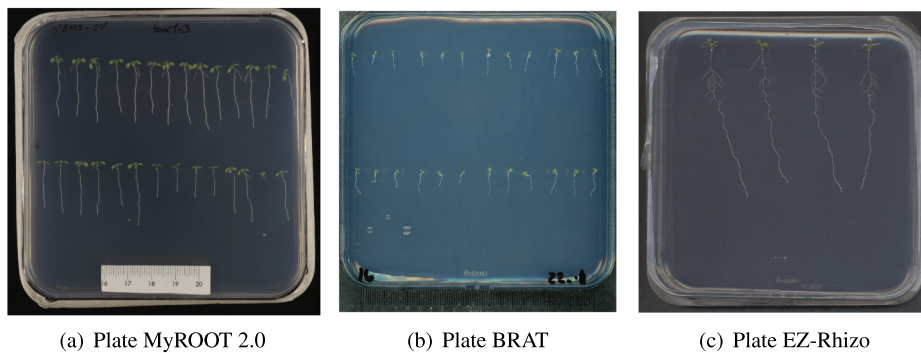


Fig. 14. The three images used for making the comparison between MyROOT 2.0, BRAT and EZ-Rhizo.

detection process.

To evaluate the hypocotyl detection process we compute the Precision-Recall (PR) curve in the three detection scenarios. Figs. 13(a), (b) and (c) present the PR curves obtained for the only wild-type, only mutant, and mutant plus wild-type hypocotyl detection experiments. The legends of each figure show the average precision obtained by each trained model (see Fig. 14).

It can be observed that the benefit obtained from using detection models specifically based on a particular type of hypocotyls is variable. On the one hand, the highest average precision obtained when detecting mutant hypocotyls is obtained when the detector is trained on only-mutant positive examples (see Fig. 13(b)). On the other hand, the best performance attained when detecting wild-type hypocotyls is given by the wild-type plus mutant detector (see Fig. 13(a)). This result is probably caused by the inherent appearance variability of wild-type hypocotyls, while their mutant counterparts show more uniform morphological traits.

However, it is not unusual to have mixed types of hypocotyls on a single plate. Thus, it makes sense to conduct an experiment that aims to detect hypocotyls of any class. The PR curves corresponding to this experiment are presented in Fig. 13(c). In this case, using a detector trained on both mutant and wild-type hypocotyls yields the highest average precision, outperforming specific models by more than 4%.

4.5. Root measurement

To finally validate the proposed framework, this experiment compares the performance of MyROOT 2.0 with other available software tools. For this reason, we compare manual measurements to those obtained by MyROOT 2.0 and two state-of-the-art root length measurement software tools: BRAT and EZ-Rhizo.

Manual measurements were made using the *Segmented line* option in ImageJ. Each root was tracked by clicking several times from the starting point of the root to the root tip. Then, the length of the segmented line was measured and ImageJ obtained the root length in millimeters using the scale set as described in Section 4.2.

In Betegon-Putze et al. (2019), this comparison was made on a set of images taken by our team of plant scientists. In contrast, to make this comparison totally unbiased and more challenging, in this study we used three images: one taken by our team of plant scientists (Fig. 14(a), containing 28 roots), and the example images provided with the BRAT and EZ-Rhizo software tools (Figs. 14(b) and (c)), containing 24 and 4 roots, respectively. Thus, we ensure that the testbed includes images deemed as ideal for test by the authors of the mentioned software tools.

First, we compare the ability of the three software tools to correctly detect roots. Table 2 shows the number and percentage of roots correctly detected by each software on each plate. It can be observed that MyROOT 2.0 and EZ-Rhizo are capable of detecting most roots (94.6% and 89.3%, respectively), while BRAT shows a really low root detection accuracy (69.6%) when applied on images the illumination conditions

Table 2

Comparison between MyROOT 2.0, BRAT and EZ-Rhizo in terms of root detection accuracy (number and percentage of detected roots).

	MyROOT 2.0	BRAT	EZ-Rhizo
Plate MyROOT 2.0	26/28 (92.9%)	15/28 (53.6%)	22/28 (78.6%)
Plate BRAT	24/24 (100%)	24/24 (100%)	24/24 (100%)
Plate EZ-Rhizo	3/4 (75%)	0/4 (0%)	4/4 (100%)

of which differ from those considered ideal for its configuration. Moreover, BRAT offers no controls (unlike MyROOT 2.0 and EZ-Rhizo) to tune the parameters that control root detection, so little can be done if it fails at detecting roots.

And second, we compare the accuracy of the root length measurements offered by the three softwares. As a ground truth, we used the manual measurements by an expert plant scientist in our team. Table 3 presents the average absolute differences between the manual measurements of all the roots in each plate and the measurements yielded by each software tool. It can be observed that MyROOT 2.0 offers by far the highest accuracy on the MyROOT 2.0 and EZ-Rhizo plates, while achieving nearly equal accurate measurements as BRAT on the BRAT plate. If the average absolute error is computed over all the set of roots in the test bed, MyROOT 2.0 attains 0.62 mm error, while this error is as high as 3.43 mm and 3.05 mm for BRAT and EZ-Rhizo, respectively. For a detailed view of the individual root length measurements, please refer to Appendix A.

These results indicate that MyROOT 2.0 is a truly useful to obtain accurate primary root length measurements in an automatic manner. While it is fair to say that BRAT is really accurate at measuring roots, it is also true that it has a high root detection error rate. On the other hand, EZ-Rhizo provides little accurate measurements when compared to MyROOT 2.0. This is due to the fact that the hypocotyl detection module based on visual appearance models of MyROOT 2.0 allows to adjust the root measurement to its true limits. In contrast, EZ-Rhizo includes a very simple hypocotyl detection step based on color, which does not improve the accuracy of its measurements.

5. Discussion

Plant phenotyping is current topic of debate with a wide range of

Table 3

Comparison between MyROOT 2.0, BRAT and EZ-Rhizo in terms of root length measurement accuracy with respect to manual measurements (average absolute measurement error in millimeters).

	MyROOT 2.0	BRAT	EZ-Rhizo
Plate MyROOT 2.0	0.38	7.98	2.66
Plate BRAT	0.79	0.59	3.30
Plate EZ-Rhizo	1.35	–	3.78

Table 4

Manual vs. MyROOT 2.0, BRAT and EZ-Rhizo root length measurements (all values in millimeters).

ID	Manual	MyROOT 2.0	BRAT	EZ-Rhizo
MR1	24.182	23.630	15.913	24.680
MR2	22.519	22.896	0.139	22.460
MR3	25.546	25.886	—	—
MR4	20.188	20.615	10.800	23.630
MR5	24.077	24.500	—	—
MR6	19.801	19.709	—	23.100
MR7	24.183	24.240	—	27.730
MR8	24.550	24.172	—	26.600
MR9	26.399	25.627	0.112	28.560
MR10	22.051	21.829	—	—
MR11	21.212	21.082	—	27.160
MR12	24.734	24.842	—	33.160
MR13	20.613	20.864	15.227	22.820
MR14	19.293	—	—	—
MR15	18.665	19.469	—	19.840
MR16	19.772	20.690	2.236	21.080
MR17	21.525	21.757	22.942	23.530
MR18	21.154	21.282	—	23.850
MR19	16.187	17.109	—	15.890
MR20	24.471	25.328	9.394	27.610
MR21	12.127	12.455	12.341	—
MR22	9.412	9.608	8.798	7.390
MR23	11.384	11.477	10.396	13.690
MR24	10.594	10.332	10.000	—
MR25	18.445	18.417	—	22.120
MR26	21.682	21.068	10.945	24.540
MR27	1.565	—	1.469	3.980
MR28	19.425	19.708	20.158	22.310
BR1	7.54	7.855	6.379	10.80
BR2	3.58	3.607	3.397	6.21
BR3	6.93	7.011	6.339	9.71
BR4	3.94	5.693	3.103	7.06
BR5	2.51	3.952	1.549	4.03
BR6	5.29	6.450	4.788	8.01
BR7	8.12	8.783	8.389	12.64
BR8	5.28	6.924	5.099	10.51
BR9	6.17	7.283	6.285	9.68
BR10	9.6	9.761	10.143	13.83
BR11	7.89	8.816	8.184	10.50
BR12	9.81	10.380	10.403	13.51
BR13	9.55	9.601	8.365	12.62
BR14	4.72	3.687	3.903	7.90
BR15	6.24	6.671	5.867	9.82
BR16	8.39	9.728	8.107	11.61
BR17	5.23	7.233	4.804	8.42
BR18	4.54	5.907	6.292	7.66
BR19	9.28	10.095	8.446	13.03
BR20	9.26	9.643	8.540	11.99
BR21	6.98	6.202	7.229	10.32
BR22	8.85	9.193	9.381	11.93
BR23	8.92	9.282	8.404	12.40
BR24	10.09	9.904	10.409	13.73
EZ1	69.43	70.944	—	73.87
EZ2	63.77	63.87	—	65.90
EZ3	66.29	68.738	—	70.42
EZ4	63.58	—	—	67.98

agricultural applications. Among all plant organs, the root is essential for overall plant growth and development. Plant scientists have long used the primary root of *Arabidopsis* as a developmental model due to its simple and stereotyped cell type organization, as its length is a phenotypic trait related to key aspects of plant growth and viability with valuable implications in agriculture.

To reduce the human effort required for measuring the length of the primary root of *Arabidopsis* seedlings grown on agar plates in laboratory conditions, this work has introduced MyROOT 2.0, an automatic tool designed jointly by computer vision and plant biology experts.

When evaluating its ability to infer image scale, MyROOT 2.0 attains subpixel precision to determine the correspondence between pixels and centimeters, analyzing to that end a segment of measuring tape placed on the plate lid. This avoids setting strict requirements in

the image acquisition process. Moreover, it is also capable of detecting the regions of the image where the roots are arranged without user supervision.

To increase the accuracy of root length measurement, MyROOT 2.0 includes an object detection module trained to find the starting points of the roots, i.e. the hypocotyls. Due to the morphologic differences that the expression of different genes may cause on the appearance of hypocotyls, different color and appearance models have been employed and tested to detect the hypocotyls. The conducted experiments indicate that training the detector with both mutant and wild-type hypocotyls yields the highest average detection precision, thus accommodating appearance variations due to genetic causes.

When comparing the manual root length measurements made by expert plant scientists and those obtained automatically via MyROOT

2.0, average differences below 1 mm are found over nearly 300 individual root measurements, which is a satisfactory result considering the huge savings in manual labor derived from using MyROOT 2.0.

Finally, the comparison between MyROOT 2.0 and two well-established state-of-the-art root length measurement software tools (BRAT and EZ-Rhizo) reveals that our proposal outperforms its competitors in terms of root detection and length measurement accuracies, achieving error measurements four to five times smaller.

All these features, coupled with its ability to process batches of images, makes MyROOT 2.0 a very appealing tool to perform high throughput automatic root phenotyping.

It is important to highlight that the involvement of plant scientists in the development loop of MyROOT 2.0 has made its usability a priority. For this reason, we have minimized the number of parameters adjustable by the user, leaving only those directly related with the image appearance (lighting condition, contrast) or the post processing of detected roots (e.g. root length filtering) available for the user to be set manually. All the many other parameters involved in the image processing pipeline (measuring tape detection, ROIs detection, root mask generation and root tracking, hypocotyl detection) have been set for a robust and optimal performance. By doing so, we have obtained a software tool that is highly usable for a wide range of images with different acquisition conditions.

Further research will be oriented towards the development of a day-by-day root growth monitoring algorithm that, starting from the detection of the hypocotyl, allows to detect abnormal root growth patterns. Our future plan also contemplates the incorporation of additional root architecture traits beyond primary root length, such as detecting branching points and measuring secondary roots. This will be important for the high throughput analysis of overall root system architecture

Appendix A. Manual vs. MyROOT 2.0, BRAT and EZ-Rhizo root length measurements

This section presents the individual root length measurements corresponding to the experiment described in Section 4.5. In particular, Table 4 presents the root length measurements obtained manually, via MyROOT 2.0, BRAT and EZ-Rhizo. Each row corresponds to an individual root, which is identified by an ID comprising two capital letters (MR, BR or EZ, to indicate if it belongs to the MyROOT 2.0, BRAT or EZ-Rhizo plate) and a number.

References

- Armengaud, P., Zambaux, K., Hills, A., Sulpice, R., Pattison, R., Blatt, M., Amtmann, A., 2009. Ez-rhizo: Integrated software for the fast and accurate measurement of root system architecture. *Plant J.* 57, 945–956.
- Arsenault, J., Pouleur, S., Messier, C., Guay, R., 1995. Winrlzo: A root measuring system with a unique overlap correction method. *HortScience* 30 (4), 906.
- Benoit, L., Rousseau, D., Belin, E., Demilly, D., Ducournau, S., Chapeau-Blondeau, F., Dürr, C., 2013. Locally oriented anisotropic image diffusion: application to phenotyping of seedlings. In: Proc. 8th International Joint Conference on Computer Vision, Imaging and Computer Graphics Theory and Applications.
- Betegon-Putze, I., González, A., Sevillano, X., Blasco-Escámez, D., Caño-Delgado, A.I., 2019. Myroot: A method and software for the semi-automatic measurement of primary root length in arabidopsis seedlings. *Plant J.* 98 (6), 1145–1156. <https://doi.org/10.1111/tpj.14297>.
- Cai, J., Zeng, Z., Connor, J.N., Huang, C.Y., Melino, V., Kumar, P., Miklavcic, S.J., 2015. Rootgraph: a graphic optimization tool for automated image analysis of plant roots. *J. Exp. Bot.* 66 (21), 6551–6562.
- Clark, R., Famoso, A., Zhao, K., Shaff, J., Craft, E., Bustamante, C., McCouch, S., Aneshansley, D., Kochian, L., 2013. High-throughput two-dimensional root system phenotyping platform facilitates genetic analysis of root growth and development. *Plant Cell Environ.* 36, 454–466.
- Dalal, N., Triggs, B., 2005. Histograms of oriented gradients for human detection. In: CVPR, San Diego, CA, USA.
- Dresboll, D., Thorup-Kristensen, K., McKenzie, B., Dupuy, L., Bengough, A., 2013. Timelapse scanning reveals spatial variation in tomato (*solanum lycopersicum* l.) root elongation rates during partial waterlogging. *Plant Soil* 369, 467–477.
- Fàbregas, N., Lozano-Elena, F., Blasco-Escámez, D., Tohge, T., Martínez-Andújar, C., Albacete, A., Osorio, S., Bustamante, M., Riechmann, J.L., Nomura, T., et al., 2018. Overexpression of the vascular brassinosteroid receptor bri1 confers drought resistance without penalizing plant growth. *Nat. Commun.* 9 (1), 4680.
- French, A., Ubeda-Tomás, S., Holman, T., Bennett, M., Pridmore, T., 2009. High-throughput quantification of root growth using a novel image-analysis tool. *Plant Physiol.* 150, 1784–1795.
- Galkovskyi, T., Mileyko, Y., Bucksch, A., Moore, B., Symonova, O., Price, C., Topp, C., Iyer-Pascuzzi, A., Zurek, P., Fang, S., Harer, J., Benfey, P., Weitz, J., 2012. Gia roots: software for the high throughput analysis of plant root system architecture. *BMC Plant Biol.* 12 (1), 116.
- Isard, M., Blake, A., 1998. Condensation: conditional density propagation for visual tracking. *IJCV* 29, 5–28.
- Iyer-Pascuzzi, A., Symonova, O., Mileyko, Y., Hao, Y., Belcher, H., Harer, J., Weitz, J., Benfey, P., 2010. Imaging and analysis platform for automatic phenotyping and trait ranking of plant root systems. *Plant Physiol.* 152 (1), 1148–1157.
- Kuijken, R.C., van Eeuwijk, F.A., Marcelis, L.F., Bouwmeester, H.J., 2015. Root phenotyping: from component trait in the lab to breeding. *J. Exp. Bot.* 66 (18), 5389.
- Kumar, P., Huang, C., Cai, J., Miklavcic, S., 2014. Root phenotyping by root tip detection and classification through statistical learning. *Plant Soil* 380 (1), 193–209.
- Le Bot, J., Serra, V., Fabre, J., Draye, X., Adamowicz, S., Pagès, L., 2010. Dart: a software to analyse root system architecture and development from captured images. *Plant Soil* 326 (1), 261–273.
- Lobet, G., Pagès, L., Draye, X., 2011. A novel image-analysis toolbox enabling quantitative analysis of root system architecture. *Plant Physiol.* 157 (1), 29–39.
- Mühlich, M., Truhn, D., Nagel, K., Walter, A., Scharr, H., Aach, T., 2008. Measuring plant root growth. In: Proc. 30th DAGM Symposium, pp. 497–506.
- Naeem, A., French, A.P., Wells, D.M., Pridmore, T.P., 2011. High-throughput feature counting and measurement of roots. *Bioinformatics* 27 (9), 1337.
- Nagel, K., Kastenholz, B., Jahnke, S., van Dusschoten, D., Aach, T., Mühlich, M., Truhn, D., Scharr, H., Terjung, S., Walter, A., Schurr, U., 2009. Temperature responses of roots: impact on growth, root system architecture and implications for phenotyping. *Funct. Plant Biol.* 36, 947–959.
- Pound, M.P., French, A.P., Atkinson, J.A., Wells, D.M., Bennett, M.J., Pridmore, T., 2013. Rootnav: Navigating images of complex root architectures. *Plant Physiol.* 162 (4), 1802–1814.
- Remler, L., Clairmont, L., Rolland-Lagan, A., Guinel, F., 2014. Standardized mapping of nodulation patterns in legume roots. *New Phytol.* 202, 1083–1094.
- Ristova, D., Rosas, U., Krouk, G., Ruffel, S., Birnbaum, K.D., Coruzzi, G.M., 2013. Rootscape: A landmark-based system for rapid screening of root architecture in arabidopsis. *Plant Physiol.* 161 (3), 1086–1096.
- Schindelin, J., Rueden, C., Hiner, M., Elcein, K., 2015. The ImageJ ecosystem: an open

traits in both plant biology and agricultural phenotyping.

Software download

MyROOT 2.0 is available for download at <https://bit.ly/2NtQDZB>.

Author contributions

A.G., M.F. and X.S. developed the algorithms for the method. A.G., X.S., I.B.-P. and D.B.-E. performed the validation experiments. I.B.-P. and D.B.-E. acquired the dataset. X.S. and A.I.C.-D. designed and supervised the study. X.S. and A.G. wrote the manuscript, and X.S., A.I.C.-D. and I.B.-P. edited the manuscript until publication.

Funding

A.I.C.-D. is a recipient of a BIO2016-78955 grants from the Spanish Ministry of Economy and Competitiveness and a European Research Council, ERC Consolidator Grant (ERC-2015-CoG - 683163). I.B.-P. is funded by the FPU15/02822 grant from the Spanish Ministry of Education, Culture and Sport. D.B.-E. is contracted with the BIO2016-78955 grant in the A.I.C.-D laboratory. CRAG is funded by “Severo Ochoa Programme” from Centers of Excellence in R&D 2016–2019 (SEV-2015-485 0533).

Declaration of Competing Interest

The authors declare that they have no known competing financial interests or personal relationships that could have appeared to influence the work reported in this paper.

- platform for biomedical image analysis. *Mol. Reprod. Dev.* 82 (7–8), 518–529.
- Slovak, R., Goschl, C., Su, X., Shimotani, K., Shiina, T., Busch, W., 2014. A scalable open-source pipeline for large-scale root phenotyping of *Arabidopsis*. *Plant Cell* 26, 2390–2403.
- Wasson, A., Richards, R., Chatrath, R., Misra, S., Prasad, S., Rebetzke, G., Kirkegaard, J., Christopher, J., Watt, M., 2012. Traits and selection strategies to improve root systems and water uptake in water-limited wheat crops. *J. Exp. Bot.* 63, 3485–3498.
- Wells, D.M., French, A.P., Naeem, A., Ishaq, O., Traini, R., Hijazi, H., Bennett, M.J., Pridmore, T.P., 2012. Recovering the dynamics of root growth and development using novel image acquisition and analysis methods. *Philos. Trans. Roy. Soc. B: Biol. Sci.* 367 (1595), 1517–1524.
- Wetterstrand, K., 2014. DNA Sequencing Costs: Data from the NHGRI Genome Sequencing Program (GSP), <http://www.genome.gov/sequencingcosts> (last accessed on September 2017).
- Wu, J., Wu, Q., Pagès, L., Yuan, Y., Zhang, X., Du, M., Tian, X., Li, Z., 2018. Rhizochamber-monitor: a robotic platform and software enabling characterization of root growth. *Plant Methods* 14 (1), 44.
- Yazdanbakhsh, N., Fisahn, J., 2007. Development of a robot-based platform applied to simultaneous root growth profiling of seedlings growing in a petri dish. In: Proc. 8th WSEAS Int'l Conference on Mathematics and Computers in Biology and Chemistry, pp. 69–73.
- Yazdanbakhsh, N., Fisahn, J., 2009. High throughput phenotyping of root growth dynamics, lateral root formation, root architecture and root hair development enabled by PlaRoM. *Funct. Plant Biol.* 36, 938–946.
- Ytting, N., Andersen, S., Thorup-Kristensen, K., 2014. Using tube rhizotrons to measure variation in depth penetration rate among modern north-european winter wheat (*Triticum aestivum* L.) cultivars. *Euphytica* 199, 233–245.